www.sciencemag.org/cgi/content/full/329/5991/553/DC1

Supporting Online Material for

Steric Effects in the Chemisorption of Vibrationally Excited Methane on Ni(100)

Bruce L. Yoder, Régis Bisson, Rainer D. Beck*

*To whom correspondence should be addressed. E-mail: rainer.beck@epfl.ch

Published 30 July 2010, *Science* **329**, 553 (2010)
DOI: 10.1126/science.1191751

This PDF file includes:

Steric effects in the chemisorption of vibrationally excited methane on Ni(100)

Bruce L. Yoder, Régis Bisson, and Rainer D. Beck
Laboratoire de Chimie Physique Moléculaire
Ecole Polytechnique Fédérale de Lausanne, Switzerland

Supporting online material

Materials and Methods

The reported experiments were performed using a triply differentially pumped continuous supersonic molecular beam source coupled to an ultra-high vacuum (UHV) surface scattering chamber (*S1*) with base pressure of 5 x 10^{-11} mbar. Gas mixtures were prepared by seeding CH_4 (99.9995% purity) or CD_3H (98% purity) in H_2 (99.9999% purity) or He (99.9999% purity). Prior to being expanded, the gas mixtures were passed through a getter trap (Supelpure-O, Supelco) in order to remove residual H_2O, O_2, CO and hydrocarbon impurities. A molecular beam was isolated using a 1 mm diameter skimmer from a supersonic jet expansion formed by expansion through a temperature controlled 50 μm diameter nozzle using 3 bar of backing pressure.

All $CD_3H(\nu_1)$ reactivity measurements used a nominal gas mixture of 3.6% CD_3H in He with a nozzle temperature of 373 K resulting in a molecular beam speed of 1895±19 m/s or translational energy of 34 kJ/mol. $CH_4(\nu_3)$ depositions employed a nominal gas mixture of 12% CH_4 in H_2 with a nozzle temperature of 323 K. These conditions produced a molecular beam with velocity of 2056±21 m/s or translational energy of 34 kJ/mol. The molecular beam impinged at normal incidence on a nickel single crystal sample cut to within 0.1° of its (100) plane. Before each deposition experiment, the Ni(100) surface was cleaned by a combination of Ar^+ ion sputtering (1000 eV kinetic energy) and annealing to 1000 K. The surface cleanliness was verified by Auger electron spectroscopy. All molecular beam deposition experiments were conducted at a surface temperature of 473 K.

Quantum state-preparation and alignment of methane was done by excitation of specific rovibrational transitions with 500-1000 mW of single mode continuous-wave infrared light near 3.3 μm generated as the idler output of a tunable optical parametric oscillator (Argos model 2400, Lockheed Martin Aculight Corp.). 10-20% of the infrared power was split off and retro-reflected through a 1.6 m absorption cell filled with 30-100 μbar of methane (CH_4 or CD_3H) in order to detect a Doppler free saturation feature (*S2*) (Lamb dip) which was used for stabilization of the OPO frequency. By locking to the 1.5 MHz FWHM Lamb dip, the laser frequency was actively stabilized to better than 1 MHz in order to maintain resonance with a rovibrational transition in the molecular beam. The remaining OPO idler power was used to excite methane molecules in the molecular beam by rapid adiabatic passage (RAP) (*S3*). The long term stability (> 1 hour) of the

frequency stabilization was verified by an IR wavemeter and by detecting the laser excited methane molecules in the molecular beam using a pyroelectric detector.

Fig. S1 shows the optical setup for excitation of the molecular beam. Nearly complete inversion of a given infrared transition can be achieved by rapid adiabatic passage with appropriate focusing of the laser beam through the molecular beam. The curved wavefronts of the focused laser beam lead to a Doppler tuning experienced by the molecules in the molecular beam as they traverse the laser beam. The rate and magnitude of the Doppler tuning can be manipulated by the choice of focal length and position of the cylindrical lens (Fig.1). We use a cylindrical lens with +25.4 cm focal length placed at a distance of 36 cm from the molecular beam. We determined the initial rotational population in the 12% CH_4 in H_2 molecular beam to be 31% in J=0, 45-52% in J=1 and 17-22% in J=2 from the asymptotic pyroelectric detector signal at high excitation laser power which corresponds to a rotational temperature of 12±3 K. The magnitude of the Doppler tuning is sufficient to induce RAP for all Doppler components of the slightly diverging molecular beam (divergence ±0.27° or ±2.9 MHz for a 2000 m/s molecular beam speed). RAP leads to the complete population inversion for allowed rovibrational transitions. There are three nuclear spin isomers of CH_4, which do not interconvert on the timescale of a supersonic expansion. Therefore, the molecular beam rotational populations for complete rotational cooling for J=0, 1, and 2 are $^5/_{16}$, $^9/_{16}$, and $^2/_{16}$, respectively. This leads to a maximum ro-vibrationally excited fraction of $^5/_{16}$ and $^9/_{16}$ for the initial J"=0 and 1 states in the molecular beam excited by RAP.

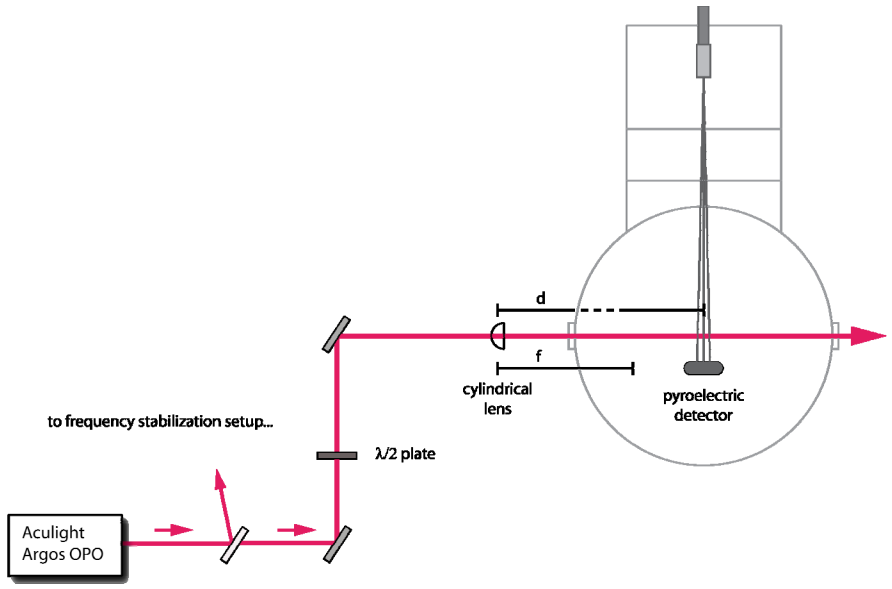

Fig. S1: Experimental setup for state-prepared, aligned molecular beam deposition experiments. For the data presented in this article, f=+25.4cm and d=36cm.

The center of the 1.4 mm wide ($1/e^2$ width) excitation region is located 1 mm from the Ni(100) surface resulting in a 500 ns time delay between the excitation/alignment and surface impact for beam speed of 2000 m/s. To ensure that the observed reactivity changes between

deposition experiments are due only to changes in the laser polarization direction, we always compare depositions done in the same run on the same clean Ni-surface. The deposition coordinates on the surface are alternated in a way to cancel out any potential local variations in surface reactivity of the nickel single crystal. We deposit up to four molecular beam spots with a footprint of 2 mm diameter each on the Ni(100) crystal of 10 mm diameter. Quantum state-resolved reaction probabilities of methane on Ni(100) were measured using Auger electron spectroscopy detection of the surface bound carbon reaction product as described previously (*S1, S4*).

Effect of nuclear hyperfine depolarization on the alignment

Measurements of the alignment contrast Δ_p as a function of distance between the excitation laser and the Ni(100) target surface (from 1 to 30 mm) show a decrease in Δ_p occurring on a timescale consistent with the hyperfine splittings of rovibrational transitions of CH_4 and CD_3H. These measurements show that for laser excitation 1 mm from the Ni(100) surface, used for all measurements except this depolarization study, hyperfine depolarization does not significantly decrease in the laser induced alignment during the 500 ns delay between excitation and surface impact for a molecular beam speed of approximately 2000 m/s.

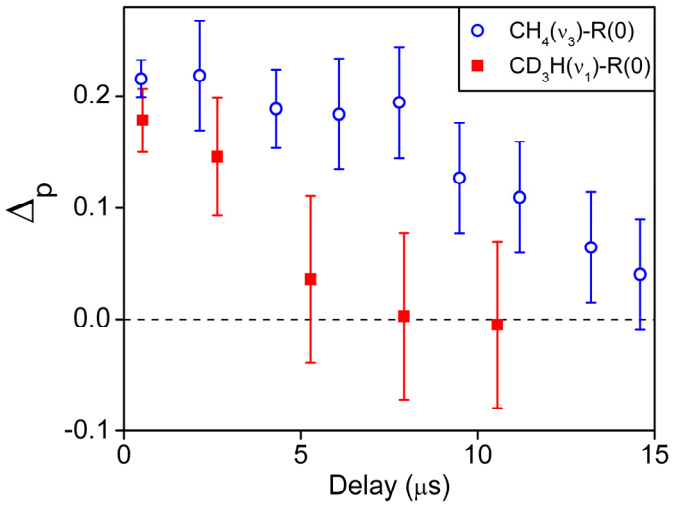

Fig. S2: Effect of hyperfine depolarization on the alignment contrast Δ_p for $CH_4(\nu_3)$ and $CD_3H(\nu_1)$ prepared by R(0) excitation. Different delay times between laser induced alignment and surface impact are realized by changing the distance between the excitation laser and target surface over a range of 1 to 30 mm. Error bars represent $\pm 2\sigma$ of the average of up to 1-9 replicate measurements.

Optical preparation of aligned reactants

Angular momentum alignment

The angular momentum $\vec{J}$ of a quantum mechanical system such as an atom or molecule is a vector quantity that can take 2J+1 orientations relative to some quantization axis given by the 2J+1 values of the magnetic quantum number M= +J, …0, …-J.

The ro-vibrational selection rules for IR-active transitions of a symmetric or spherical top molecule excited by linearly polarized radiation are:

R-branch: $\Delta J = +1$ and $\Delta M = 0$ and $\Delta K = 0$

P-branch: $\Delta J = -1$ and $\Delta M = 0$ and $\Delta K = 0$

Q-branch: $\Delta J = 0$ and $\Delta M = 0,\ M \neq 0$

and $\Delta K = 0,\ K \neq 0$

(transitions from M"=0 to M=0 are not allowed)

(transitions from K"=0 to K=0 are not allowed)

Fig. S3 shows the four rovibrational transitions used to prepare $CH_4(\nu_3)$ in our study of quantum state-specific, alignment dependent surface reactivity. $CD_3H(\nu_1)$ transitions are similar to those shown in Fig. S3, with the addition of non-degenerate K-levels for the symmetric top molecule. Here, K denotes the projection of $\vec{J}$ onto the figure axis of the symmetric top. When considering alignment of $\vec{J}$, this difference between CH_4 and CD_3H is irrelevant. For all transitions shown, except the P(1) transition, excitation by linearly polarized light prepares anisotropic M-level populations in the excited state due to the ΔM selection rules.

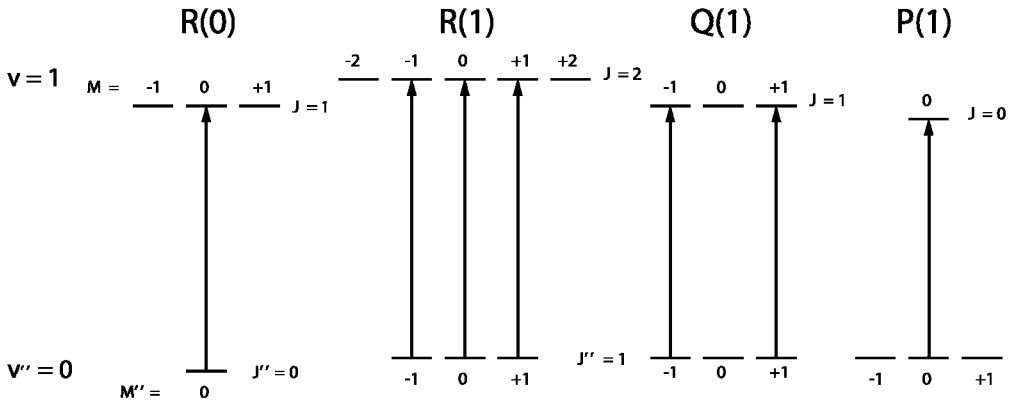

Fig. S3: Energy level diagrams for CH_4 rovibrational transitions excited by linearly polarized light.

Fig. S4 shows the $\vec{J}$ alignment produced in the vibrationally excited state by excitation via the R-, P-, and Q-branch transitions (Fig. S3). For the R(0) excitation, which produces the strongest $\vec{J}$ alignment, $CH_4(\nu_3{=}1)$ is prepared specifically in the J=1, M=0, level aligning $\vec{J}$ perpendicular to the polarization axis Z. R(1) excitation at high laser power leads to equal population in the J=2, M=0 and ±1 levels without populating the J=2, M=±2, levels. This

corresponds again to a preferential alignment of $\vec{J}$ perpendicular to the polarization axis but to a lesser degree than produced by R(0) excitation. On the other hand, Q(1) excitation populates equally the J=1, M= ±1 sublevels but transfers no population to J=1, M=0 and therefore aligns $\vec{J}$ preferentially parallel to the quantization axis. Finally, P(1) excitation prepares $CH_4(\nu_3=1)$ with J=0, M=0 the only allowed level for J=0, resulting in no alignment of $\vec{J}$.

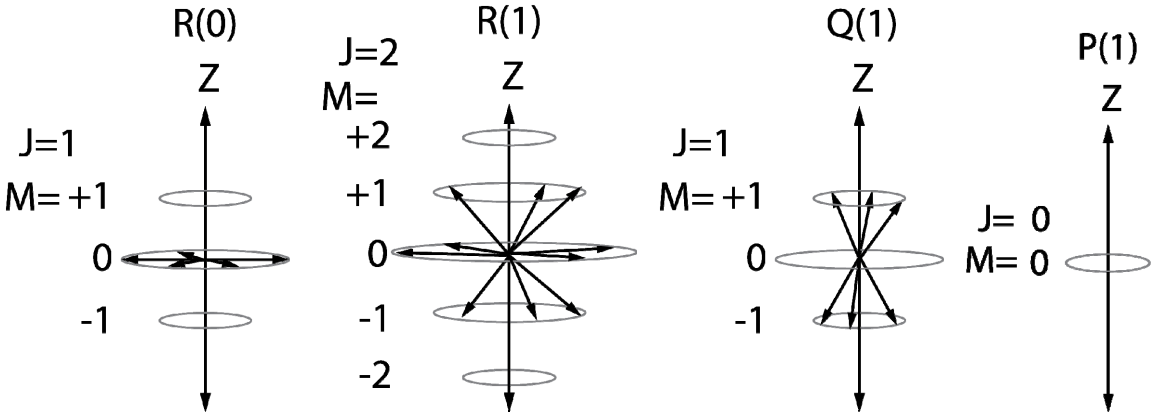

Fig. S4: Anisotropic M-level distributions produced by $CH_4(\nu_3)$ transitions used in the study of quantum state-resolved, alignment dependent reactivity.

In an oriented sample, $\vec{J}$ has a preferred direction, either parallel or antiparallel to Z, due to unequal populations of the +M and –M levels. An aligned sample is characterized by a anisotropic population of the |M| levels such that $\vec{J}$ is aligned either parallel or perpendicular to the quantization axis (Fig. S4). Excitation by linearly polarized light obeys a ΔM=0 selection rule, exciting levels with positive and negative M values indistinguishably and creates an aligned ensemble of molecules. Oriented samples of molecules can be prepared by excitation with circularly polarized light due to the ΔM= ±1 selection rule but this has not been used here.

The degree of angular momentum alignment created by linearly polarized laser excitation can be described quantitatively using the alignment coefficient $A_0^{(2)}$, which describes the ensemble average of the angle θ between $\vec{J}$ and the quantization axis:

$$A_0^{(2)} = \left\langle 3\cos^2\theta - 1 \right\rangle \qquad \text{(eq. 1S)}$$

$A_0^{(2)}$ is the second order expansion coefficient in an expansion of any cylindrically symmetric angular distribution in terms of the Legendre polynomials $P_l(\cos\theta)$:

$$P(\theta) = \frac{1}{4\pi}\sum_l A_0^{(l)} P_l(\cos\theta) \qquad \text{(eq. 2S)}$$

$A_0^{(2)}$ can take values between +2 and -1, where positive and negative values of $A_0^{(2)}$ describe an alignment parallel and perpendicular to the quantization axis, respectively. $A_0^{(2)}$ = 0 corresponds to an isotropic population of all possible M-levels resulting in no alignment. For an aligned ensemble characterized by a value of $A_0^{(2)}$, the probability of finding $\vec{J}$ at angle θ from the polarization axis is given by:

$$P_J(\theta) = \frac{1 + A_0^{(2)} \frac{1}{2}\left(3\cos^2\theta - 1\right)}{4\pi} \qquad \text{(eq. 3S)}$$

Examples of the angular distribution $P_J(\theta)$ for specific values of $A_0^{(2)}$ are shown in Fig. S5:

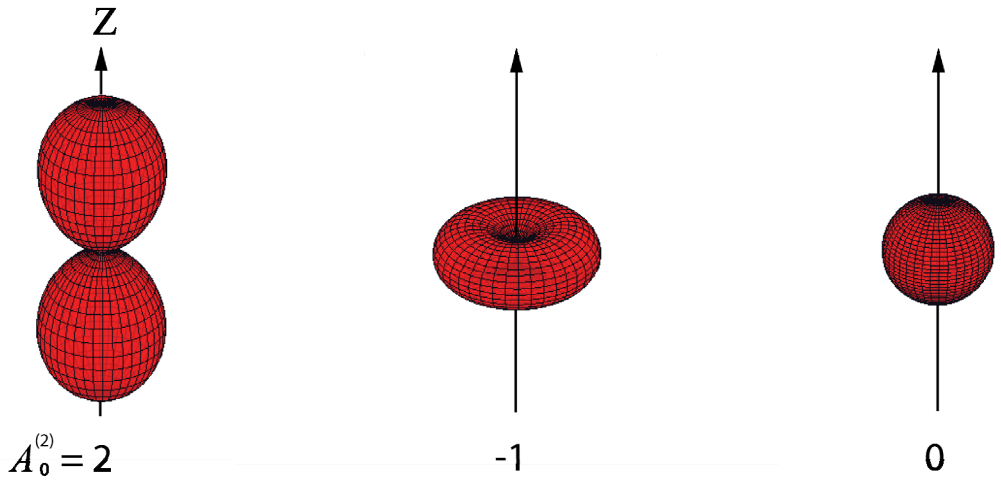

Fig. S5: Angular distributions $P_J(\theta)$ for $A_0^{(2)} = 2, -1, \text{and } 0$.

The values of $A_0^{(2)}$ describing the alignment produced by linearly polarized excitation via P-, Q-, and R-branch transitions have been calculated by Zare and others (*S5-S8*) for conditions of weak optical pumping, where the isotropic populations of the initial M"-levels is not perturbed significantly by the optical pumping. Under this condition, the calculation of the alignment coefficients $A_0^{(2)}$ reduces to a summation over all initial M"-levels, connected to the excited state, and adding the corresponding transition strength given by the Clebsch-Gordan coefficients. With increasing initial J value, the alignment produced by optical pumping results to a large part due to the differences in the transition probabilities between different initial and final M levels. For strong pumping conditions the population transfer is no longer a linear function of the transition

probability and the general calculation of the $A_0^{(2)}$ coefficients becomes more complicated because the laser power dependent M"-level populations need to be taken into account.

The condition of weak optical pumping is not satisfied in our experiments because the excitation by rapid adiabatic passage results in a complete population transfer from the initial M"-levels to the optically accessible final M-levels of the excited J-state. Fortunately, for excitation via P(1), Q(1), and R(0), the optical transitions all originate from a single |M"| level which reduces the sum over M"-levels to a single term and therefore the expressions given by Zare and coworkers remain valid for these three transitions even for strong optical pumping. In other words, the alignment produced for P(1), Q(1), and R(0) excitation is simply a result of the ΔM=0 selection rule which remains valid for excitation by rapid adiabatic passage.

For R(1) excitation with linearly polarized light, the calculation of the $A_0^{(2)}$ coefficient has to be modified for the case of strong optical pumping used in our experiments. Instead of summing the contributions from initial M" = 0 and M" = 1 levels (Fig. S3) with the corresponding transition strength given by Clebsch-Gordan coefficients ($^2/_3$ and ½ for M"=0 and $\pm$1, respectively). Assuming that each of the three transitions is excited to the same extent, we calculate

$A_0^{(2)}$ = -0.67 for strong pumping instead of $A_0^{(2)}$ = -0.70 for the case of weak pumping. The resulting angular momentum alignment coefficients for the transitions used in our experiments are shown in Fig. S6.

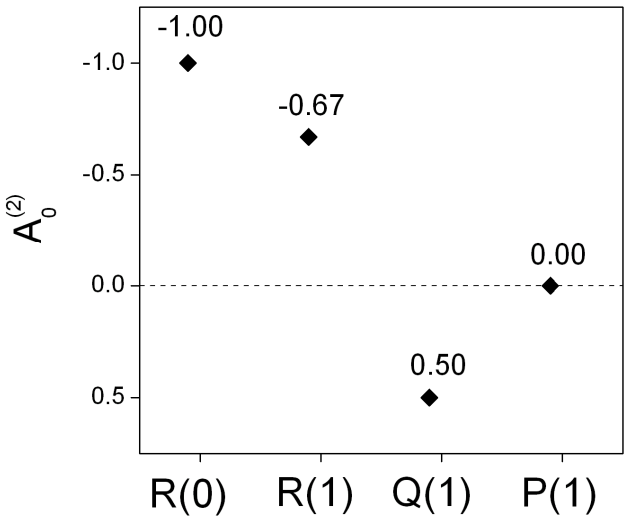

Fig. S6: Calculated alignment coefficients, $A_0^{(2)}$, valid for the different rovibrational transitions of $CH_4(\nu_3)$ and $CD_3H(\nu_1)$ used in the study of alignment dependent reactivity.

Inserting the relevant $A_0^{(2)}$ into eq. 3S, results in the probability distributions of finding $\vec{J}$ at an angle θ with respect to the linear polarization axis of the excitation laser $\vec{E}$.

Vibrational transition dipole moment alignment

Alignment of a molecule's J-vector defines the distribution of the molecule's rotational axis in space, which also leads to an alignment of the bonds and the vibrational transition dipole moment if the molecule is in a vibrationally excited state. In the simplest case of a diatom such as CO or a parallel vibration of a linear molecule, the stretched bond(s) and the vibrational transition dipole moment $\vec{\mu}_{\mathrm{if}} = \langle \psi_{\mathrm{i}} | \hat{\mu} | \psi_{\mathrm{f}} \rangle$ are parallel to each other and perpendicular to $\vec{\mathrm{J}}$. The bond alignment resulting from linearly polarized excitation of linear molecules as well as for a parallel band of a symmetric top molecule (ν_1 of CD_3H) has been calculated by Zare (*S7*, *S9*) who showed that the corresponding alignment coefficient β_{axis} can take values between +2 and 0. The probability distribution of finding the vibrational transition dipole moment or the stretch excited bond at an angle θ from the polarization axis is given by an expression identical to the J-vector alignment except that the J-vector alignment coefficient $A_0^{(2)}$ is replaced by the bond alignment coefficient β_{axis}.

$$\mathrm{P_J}(\theta) = \frac{1 + \beta_{\mathrm{axis}} \frac{1}{2}\left(3\cos^2\theta - 1\right)}{4\pi} \qquad \text{(eq. 4S)}$$

Note that in contrast to $A_0^{(2)}$, β_{axis} takes only positive values, indicating that the bond alignment and the alignment of the vibrational transition dipole moment is always in the direction of the laser polarization axis for a parallel vibration of a symmetric top. Fig. S7 shows the calculated β_{axis} values for the transitions used to probe the steric effects in the dissociative chemisorption of $CH_4(\nu_3)$.

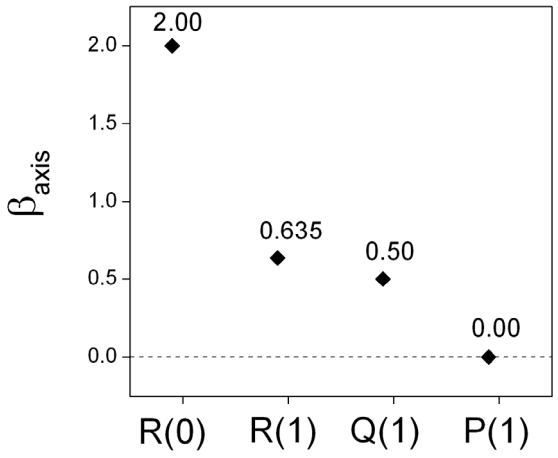

Fig. S7: Calculated alignment coefficients β_{axis} valid for the indicated ro-vibrational transitions of $CH_4(\nu_3)$ and $CD_3H(\nu_1)$ for the case of unresolved K-structure.

Here $CH_4(\nu_3)$ has been treated as a symmetric top with unresolved K-structure, as the K-levels of a given J-state are degenerate in a spherical top. The 'figure axis' of $CH_4(\nu_3)$ has been considered to be the axis containing the net vibrational C-H stretch amplitude.

For the R(1) transition of CD_3H, we also calculated β_{axis} for the case of resolved K-structure (Fig. S8), as we were able to resolve the K-structure in the excitation of $CD_3H(\nu_1)$ and excited separately transitions with J"=1, K"=0 and J"=1, K"=1.

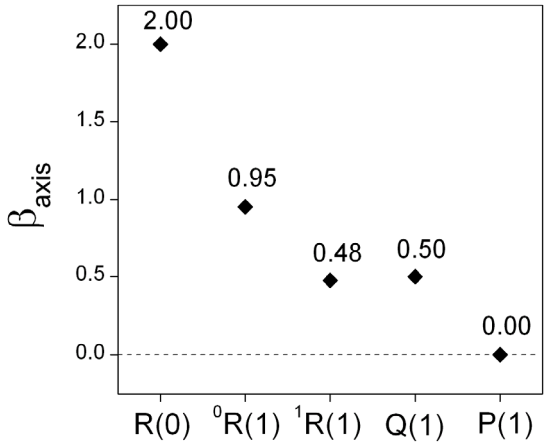

Fig. S8: Calculated alignment coefficients β_{axis}, for excitation of $CD_3H(\nu_1)$ via the rovibrational transitions with resolved K-structure.

Fig. S9 shows the reactant alignment for $CH_4(\nu_3)$ and $CD_3H(\nu_1)$ produced upon P-, Q- and R-branch excitation. The probability distribution of $\vec{J}$ with respect to the excitation's polarization $\vec{E}$ axis is given in red. The probability distribution of $\vec{\mu}_{if}$ is shown in blue. Here, the R(1) alignment presented is for the case of un-resolved K-structure.

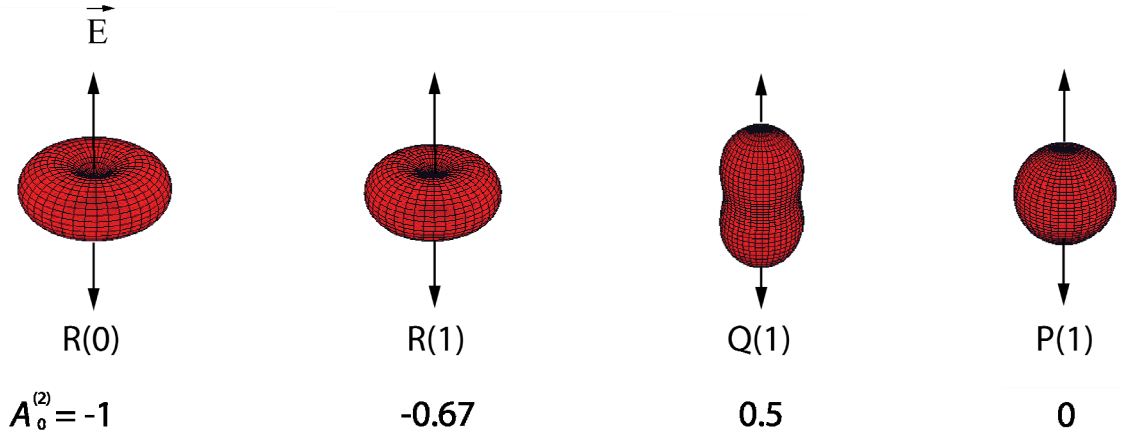

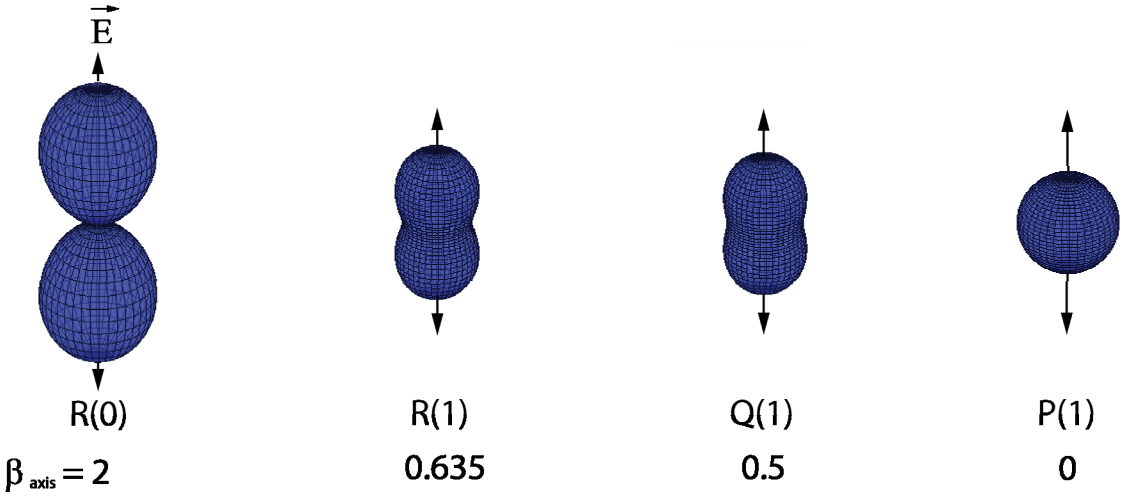

Fig. S9: Probability distribution of $\vec{J}$ (in red) and vibrational transition dipole moment (in blue). $\vec{E}$ marks the polarization axis of the excitation laser. Note the effect of the sign change in the $A_0^{(2)}$ alignment coefficient which occurs for switching from R to Q-branch. No sign change occurs for β_{axis} resulting in angular distributions aligned parallel to $\vec{E}$ for both R and Q-branch excitation.

Comparison of the measured alignment contrast Δ_p with calculated alignment coefficients $A_0^{(2)}$ and β_{axis}

Fig. S10 shows the experimentally observed alignment contrast Δ_p compared to the calculated alignment coefficients $A_0^{(2)}$ (S10(a)) and β_{axis} (S10(b)) for $CH_4(\nu_3)$ prepared via the indicated transition. The reactivity data used to calculate the Δ_p values was collected using a 34 kJ/mol translational energy molecular beam impinging at normal incidence on a Ni(100) crystal held at 200 °C. The vertical axes in Fig. S10(a) are scaled such that the origins and the values associated with R(0) excitation coincide for Δ_p and $A_0^{(2)}$. The calculated $A_0^{(2)}$ alignment coefficients change sign in switching from R-branch to Q-branch excitation. This sign change is not observed in the Δ_p.

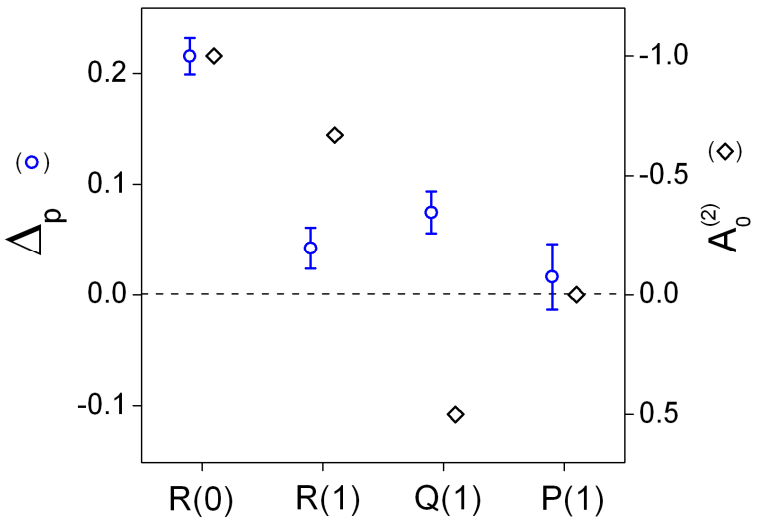

Fig. S10(a): Comparison of the experimentally determined Δ_p values for $CH_4(\nu_3)$ to the corresponding calculated $\vec{J}$ alignment coefficients $A_0^{(2)}$. Error bars represent ± 2σ of the average of 4-9 replicate measurements.

Fig. S10(b) shows the calculated alignment coefficients β_{axis} for the vibrational transition dipole moment of four $CH_4(\nu_3)$ transitions for the case of strong optical pumping versus experimentally determined values of Δ_p. The vertical axes of the graph are scaled such that the origins and the values associated with R(0) excitation coincide for Δ_p and β_{axis}.

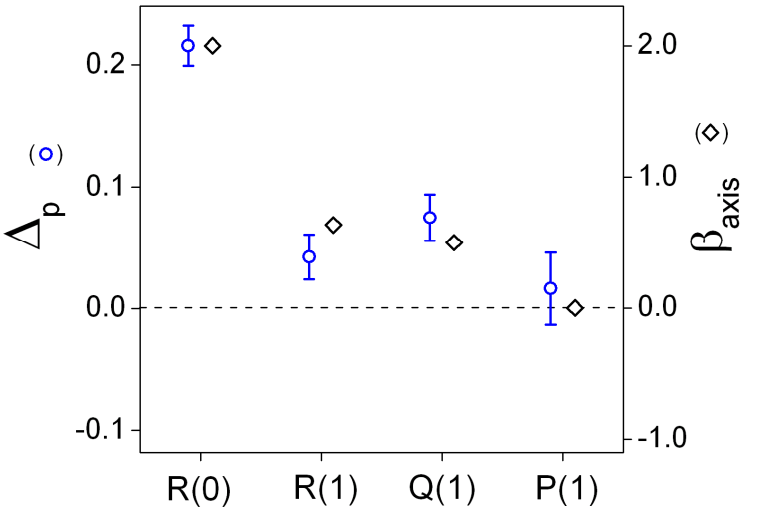

Fig. S10(b): Comparison of the experimentally determined Δ_p values for $CH_4(\nu_3)$ to the corresponding calculated vibrational transition dipole moment alignment coefficients β_{axis}. Error bars represent ± 2σ of the average of 4-9 replicate measurements.

Inspection of the calculated β_{axis} alignment coefficients in Fig. S10(b) shows that the sign of β_{axis} remains positive for both R- and Q-branch transitions. The positive β_{axis} alignment

coefficients signify a preferential alignment of the vibrational transition dipole moment (or net C-H stretch amplitude) parallel to the polarization axis of the excitation laser for both R- and Q-branches. The fact that Δ_p does not change sign (parallel polarization producing larger reactivity for R(0), R(1) and Q(1)), leads to the conclusion that the observed alignment effect is dominated by an alignment of the vibrational transition dipole moment rather than $\vec{J}$ alignment. For all transitions excited (except P(1), where Δ_p=0), a higher reactivity is observed for molecules having their vibrational transition dipole moment aligned parallel to the surface rather than perpendicular to it.

Polarization angle dependence of the $CH_4(\nu_3)$ and $CD_3H(\nu_1)$ reactivity

To obtain a detailed polarization angle dependence of the alignment effect, we measured the reactivity for a 34 kJ/mol translational energy molecular beam of $CH_4(\nu_3)$-R(0) excited at several intermediate polarization angles in addition to 0° (II-pol) and 90° (⊥-pol) measurements. Fig. S11 shows the results of these measurements. The angle dependent reactivity exhibits a monotonic decrease from parallel to perpendicular polarization.

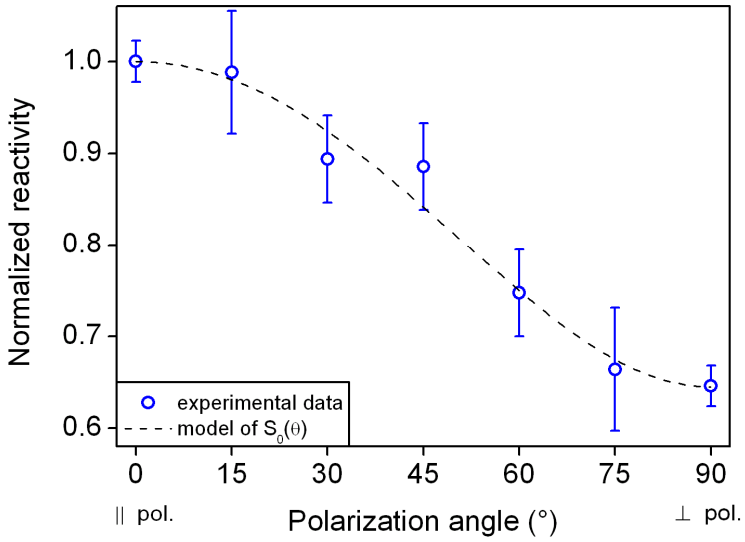

Fig. S11: Effect of laser polarization angle on the reactivity of $CH_4(\nu_3)$ on Ni(100) for R(0) excitation. The reactivity is normalized to the value measured for parallel polarization. The dashed line gives the reactivity by the geometric model described in the text. Error bars represent ± 2σ of the average of 2-9 replicate measurements.

We also measured the polarization angle dependence of reactivity for a 34 kJ/mol translational energy molecular beam of $CD_3H(\nu_1)$-R(0). Fig. S12 shows the results. The angle dependent reactivity, again, exhibits a monotonic decrease from parallel to perpendicular polarization.

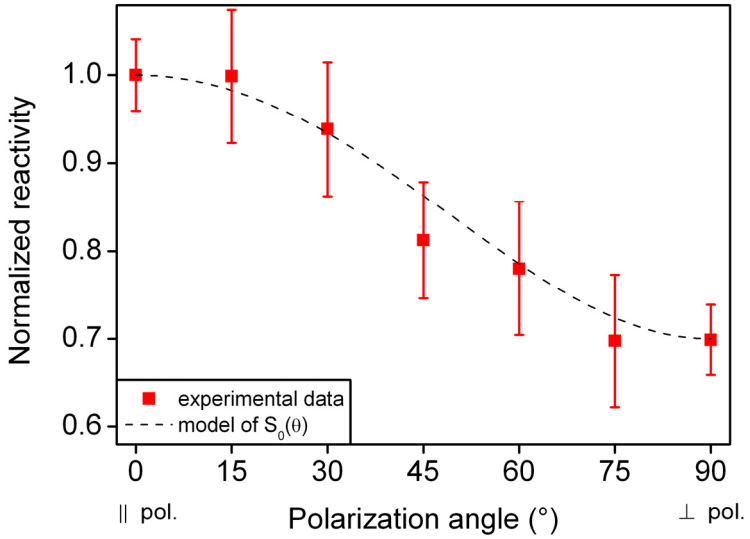

Fig. S12: Effect of laser polarization angle on the reactivity of $CD_3H(\nu_1)$ on Ni(100) for R(0) excitation. The reactivity is normalized to the value measured for parallel polarization. The dashed line gives the reactivity by the geometric model described in the text. Error bars represent $\pm 2\sigma$ of the average of 2-7 replicate measurements.

In fact, the reactivity data at intermediate angles (15° to 75°) can be predicted from the measured reactivities for parallel and perpendicular alignment $S_0^{\parallel}$ and $S_0^{\perp}$ by a simple geometric model. At any angle θ with respect to the surface plane, the angle dependent reactivity $S_0(\theta)$ is assumed to be composed of a parallel and perpendicular reactivity contributions given by $S_0^{\parallel}\sin\theta$ and $S_0^{\perp}\cos\theta$, respectively. The vector addition of the two components gives $S_0(\theta)$ as a function of $S_0^{\parallel}$, $S_0^{\perp}$ and θ:

$$S_0(\theta) = \sqrt{\left(S_0^{\parallel}\right)^2 - \sin^2\theta \cdot \left[\left(S_0^{\parallel}\right)^2 - \left(S_0^{\perp}\right)^2\right]} \qquad \text{(eq. 5S)}$$

Using the normalized reactivity of $S_0^{\parallel}$=1 and $S_0^{\perp}$=0.645 found for $CH_4(\nu_3)$-R(0) and $S_0^{\parallel}$=1 and $S_0^{\perp}$=0.70 for $CD_3H(\nu_1)$-R(0) from repeated measurements, we calculate $S_0(\theta)$ using equation 5S as function of θ (Dashed lines in Fig. S11 and S12). The measured normalized reactivities at the intermediate polarization angles agree with this functional form of $S_0(\theta)$.

References:

S1. M. P. Schmid, P. Maroni, R. D. Beck, T. R. Rizzo, *Rev. Sci. Instrum.* **74**, 4110 (2003).
S2. W. Demtröder, *Laser Spectroscopy: Basic Concepts and Instrumentation*. (Springer, Berlin, 1998).

S3. N. V. Vitanov, T. Halfmann, B. W. Shore, K. Bergmann, *Ann. Rev. Phys. Chem.* **52**, 763 (2001).
S4. R. D. Beck *et al.*, *Science* **302**, 98 (2003).
S5. C. H. Greene, R. N. Zare, *Ann. Rev. Phys. Chem.* **33**, 119 (1982).
S6. A. J. Orr-Ewing, R. N. Zare, *Ann. Rev. Phys. Chem.* **45**, 315 (1994).
S7. W. R. Simpson, T. P. Rakitzis, S. A. Kandel, A. J. Orr-Ewing, R. N. Zare, *J. Chem. Phys.* **103**, 7313 (1995).
S8. E. H. Van Kleef, I. Powis, *Mol. Phys.* **96**, 757 (1999).
S9. R. N. Zare, *Der Buns.-Ges.-Phys. Chem. Chem. Phys.* **86**, 422 (1982).